Picosecond intensity statistics of semiconductor lasers operating in the low-frequency fluctuation regime

D. W. Sukow,[1] T. Heil,[2] I. Fischer,[2] A. Gavrielides,[1] A. Hohl-AbiChedid,[1] and W. Elsäßer[2]
[1]*Nonlinear Optics Center, Air Force Research Laboratory AFRL/DELO, 3550 Aberdeen Avenue SE, Kirtland AFB, New Mexico 87117-5776*
[2]*Institut für Angewandte Physik, Technische Universität Darmstadt, Schloßgartenstraße 7, D-64289 Darmstadt, Germany*
(Received 22 January 1999)

We present detailed statistical investigations of the irregular fast pulsing behavior present in the dynamics of semiconductor lasers with delayed optical feedback operating in the low-frequency fluctuation and coherence collapse regimes. We demonstrate that the probability density distributions of the laser intensity on a picosecond time scale are essentially independent of the number of optical modes involved in the laser emission, using two complementary high-resolution experimental measurement systems: a high-bandwidth sampling digitizer and a single-shot streak camera. The experimental results are supported by numerical studies using the single-mode Lang-Kobayashi equations, as well as a multimode extension of the model. Furthermore, we also demonstrate that gain saturation and coexisting attractors can cause substantial qualitative changes of the probability density distribution. [S1050-2947(99)09507-4]

PACS number(s): 42.55.Px, 42.60.Mi, 42.65.Sf

I. INTRODUCTION

Semiconductor lasers are well known to be highly susceptible to external optical perturbations. In many common applications, the perturbation consists of delayed feedback from the laser's own field arising from a distant partial reflector, such as a fiber facet or optical disk. Systematic experimental studies of the dynamics of such systems typically use an external cavity configuration; numerical and analytical investigations often employ a set of delay-differential rate equations known as the Lang-Kobayashi (LK) model [1]. Delayed optical feedback can improve a laser's operating characteristics under some conditions, resulting in linewidth narrowing or squeezing [2,3], for example. However, over wide parameter ranges, the feedback gives rise to rich and unstable nonlinear behavior which is not yet fully understood. One particularly complex behavior that has proved challenging both experimentally and theoretically is known as low-frequency fluctuations (LFF) [4]. This phenomenon occurs when the laser is operated with moderate optical feedback from an external cavity [5], where the delay time is long compared to the period of the laser's relaxation oscillations. Historically, it has been studied near the laser threshold, but is known to exist at much higher pumping levels [6]. As the pumping level increases, the LFF regime typically gives way to coherence collapse [7].

One important aspect of LFF is the extremely wide range of time scales present in its dynamics. Figure 1 shows typical intensity time series: Fig. 1(a) shows an intensity time series 400 ns long, recorded with a digital oscilloscope with 1 GHz bandwidth low-pass filtering; Fig. 1(b) shows an unfiltered intensity time series 7 ns long, recorded under identical conditions using a single-shot streak camera with a bandwidth larger than 50 GHz. As depicted by Fig. 1(a), the sporadic intensity dropout events are typically tens of nanoseconds long, and are separated by irregular intervals which can be on the order of hundreds of nanoseconds or more. These result in increased ''noise'' in the radio frequency spectrum as observed by Risch and Voumard [4] over two decades ago. On the much shorter time scale shown in Fig. 1(b), there is an irregular train of intensity pulses within the envelope of the slower dropout events, with pulse durations on the order of 100 ps. These pulses were predicted by van Tartwijk *et al.* [8] based on numerical simulations of the LK equations, and were first observed experimentally by Fischer *et al.* [9] using a streak camera. This extraordinary range of time scales creates one of the principal challenges of LFF from both numerical and experimental points of view. Numerically, accurate simulations are difficult and computationally expensive due to the stiffness of the equations. Experimentally, data-acquisition technology does not at present allow for microsecond-length time series to be recorded with picosecond resolution, which would be needed to capture multiple

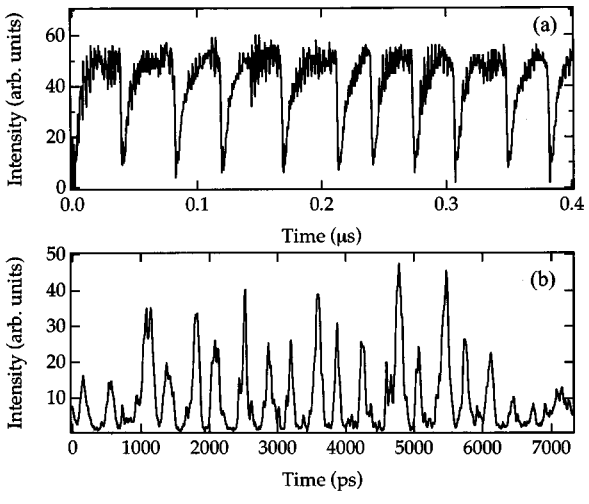

FIG. 1. Typical single-shot intensity time series of a semiconductor laser operating in the LFF regime. (a) Time series, low pass filtered with a bandwidth of 1 GHz recorded by a fast digital oscilloscope. (b) Time series recorded by a streak camera with a bandwidth of more than 50 GHz. Identical experimental conditions in (a) and (b).

dropout events and still faithfully reproduce the fast pulses. Lacking the experimental capability of performing a careful time-series analysis, several researchers have turned to statistical measurements of the dynamics on both fast and slow time scales [10–12].

Much research has been devoted to understanding the mechanism behind LFF [8–16]. A current area of debate is the issue of multiple longitudinal mode operation [17–19]. Multimode operation often occurs when the laser undergoes LFF dynamics even if the solitary laser is single mode [20]. However, LFF still persists when the laser is restricted to a single mode using a grating or an intracavity etalon. Furthermore, the LK model assumes only a single mode of operation, yet it has been the basis of many successful numerical and analytical studies of the phenomenon. Thus, the specific influence of multiple longitudinal modes in LFF remains unclear.

In this paper, we present detailed experimental and numerical studies of the statistics of the picosecond intensity pulses. We investigate if there is a difference in the intensity statistics between single-mode and multimode operation, what the effects of gain saturation are, and to what extent the LK model captures the essence of the dynamics. Following this Introduction, we review the LK equations and their approximations, and describe a multimode extension [21,22] of the model. Then, we measure experimental probability distributions for both single-mode and multimode cases in two independent experimental systems. Our results show only trivial differences in the statistics obtained for single-mode and multimode systems, a finding that is supported numerically. We also investigate the role of gain saturation, finding that it can lead to qualitatively different probability distributions. Overall, we find that the single-mode LK equations reproduce all phenomena we observe experimentally, which suggests that they retain the essence of the dynamics in this regime.

II. THEORETICAL MODELS

Semiconductor lasers subject to weak and moderate optical feedback have been modeled successfully with the Lang-Kobayashi equations [1]. These equations combine a phenomenological description of the semiconductor medium with a first-principles wave equation for the electric field. They can be expressed as dimensionless rate equations [23] for the complex electric field $\mathcal{E}$ and the excess carrier number N:

$$\frac{d\mathcal{E}}{dt}=\frac{1}{2}(1+i\alpha)[(1+2N)F(\mathcal{E})-1]\mathcal{E} + \eta\mathcal{E}(t-\tau)\exp(-i\omega_0\tau), \tag{1}$$

$$T\frac{dN}{dt}=P-N-(1+2N)F(\mathcal{E})|\mathcal{E}|^2. \tag{2}$$

In these equations, time t is measured in units of the photon lifetime τ_p, and the external round-trip time is normalized as $\tau\equiv 2L/(c\tau_p)$. The electric field amplitude E and phase ϕ are defined by $\mathcal{E}=E\exp(i\phi(t))$. The angular frequency of the solitary laser ω is expressed in dimensionless form as $\omega_0 \equiv \omega\tau_p$, η is the normalized feedback rate, and P is proportional to the pumping rate above threshold. The linewidth enhancement factor α and the ratio of the carrier to photon lifetimes $T=\tau_s/\tau_p$ characterize the semiconductor medium. The function $F(\mathcal{E})$ is a nonlinear gain correction term often included in the LK model, and usually has the form $F(\mathcal{E}) =1/(1+\epsilon|\mathcal{E}|^2)\simeq(1-\epsilon|\mathcal{E}|^2)$, with the assumption that $\epsilon|\mathcal{E}|^2 \ll 1$.

The LK equations make two important approximations. First, they assume that only a single longitudinal mode of the solitary laser is active. This is reflected in the presence of a single complex electric field $\mathcal{E}$. Second, they are designed for weak or moderate feedback, so terms of order η^2 or higher, corresponding to multiple external cavity round-trips, are assumed to be negligible. However, multiple round-trip terms can easily be appended if it is found that they are important.

The multimode generalization of the LK equations incorporates additional optical modes that are coupled through the carrier inversion in a manner similar to that described in Ref. [24]. The equations for this expanded system, again given in dimensionless form, are

$$\frac{d\mathcal{E}_i}{dt}=\frac{1}{2}(1+i\alpha)[(1+2N)F_i(\mathcal{E})-\delta_i]\mathcal{E}_i + \eta_i\mathcal{E}_i(t-\tau)\exp(-i\omega_i\tau), \tag{3}$$

$$T\frac{dN}{dt}=P-N-(1+2N)\sum_i |\mathcal{E}_i|^2F_i(\mathcal{E}), \tag{4}$$

where $\mathcal{E}_i$ is the complex electric field of the ith solitary laser mode with a dimensionless angular frequency ω_i. Each mode may be assigned different feedback coefficients η_i and losses δ_i. The gain is linearized about transparency, and self- and cross-saturation terms are taken into account through the term $F_i(\mathcal{E})$, which has the form

$$F_i(\mathcal{E})=1-k|\mathcal{E}_i|^2-\sum_j \beta_{ij}|\mathcal{E}_j|^2. \tag{5}$$

In Eq. (5), k is the mode-independent self-saturation, and β_{ij} is the cross-saturation matrix. Note that the *total* self-saturation for the ith mode is given by the sum of k and β_{ii}, the corresponding diagonal element of the cross-saturation matrix. The cross-saturation matrix elements have the form

$$\beta_{ij}=C\frac{1+\alpha\tau_{\rm pol}\Delta\Omega(i-j)}{1+[\tau_{\rm pol}\Delta\Omega(i-j)]^2}, \tag{6}$$

where $\tau_{\rm pol}\sim 0.1$ ps has been identified with the polarization relaxation time, α with the linewidth enhancement factor, and $\Delta\Omega$ is the solitary laser longitudinal line separation [25,26]. There remains some controversy [25] regarding the correct physical interpretations and values for α and $\tau_{\rm pol}$, but experiments tend to favor this particular identification [27]. The prefactor C in Eq. (6) is derived from a density-matrix calculation [25], but has substantial variability due to phenomenological parameters such as the spatial mode overlap, for example. All other terms in Eqs. (3) and (4) have the same meanings as in the single-mode LK model.

We use the single-mode and multimode LK models for numerical investigations of the intensity statistics, with typical sets of parameters: $\tau_p=1.0$ ps, $\tau_s=1.5$ ns, $T=1500$, $\tau=1500$, $\alpha=5$, and $\omega_0\tau=-1$. The values for the pumping

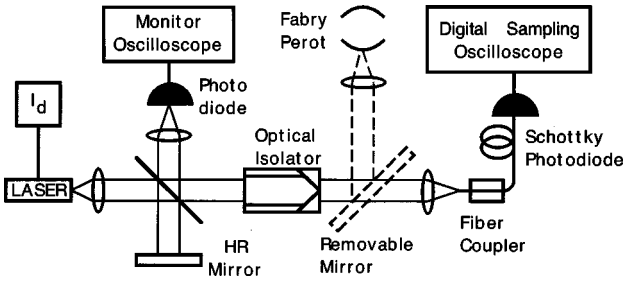

FIG. 2. Setup for the fast sampling oscilloscope experiment.

rate and threshold reduction correspond to the experimental conditions. The external cavity length associated with this parameter set is $L=24.5$ cm. For multimode calculations, we assume $i=5$ active optical modes (based on experimental observations), and that all modes have equal losses (δ_i). We also make the approximation that all modes have equal gains, although a parabolic shape for the gain profile could be added with a term such as $b(\lambda_i-\lambda_o)^2$. The value of the cross-coupling strength C is set such that it contributes 28% of the *total* modal self-saturation, although our numerical results do not depend sensitively on this value. We use a fourth-order Runge-Kutta algorithm for numerical integration of Eqs. (1)–(4). Numerical results will be shown in Sec. IV in direct comparison with experimental findings.

III. EXPERIMENTAL APPARATUS

We perform two independent experiments, using different and complementary data-acquisition systems. One experiment uses a digital sampling scope, which has the advantage of recording a very large number of truly random sampled data points of the LFF intensity dynamics. The other uses a streak camera, which has very high sensitivity and bandwidth that can be used to probe accurately the near-threshold regime. The configurations for these two systems are shown in Figs. 2 and 3, and the details of the experiments are described in the following sections.

A. Fast sampling scope experiment

In the experiment depicted in Fig. 2, we use a temperature-stabilized laser diode (Sharp LT015MD), a double heterojunction laser in a V-channeled substrate inner stripe structure. This laser operates at a nominal wavelength of $\lambda=830$ nm and has a threshold current of $J_{\rm th}=41.3$ mA. An aspheric lens (Thorlabs C110TM-B, numerical aperture $=0.4$) collimates the beam. A beamsplitter directs 30% of the light to a high-reflectivity mirror which forms the external cavity; the distance between the laser and this mirror is 22 cm. The remaining 70% of the light passes through a Faraday isolator (OFR-5-NIR) and is coupled to a multimode fiber-coupled Schottky photodetector with a 25 GHz bandwidth (New Focus 1434-50). We connect the 25 GHz detector to a Communications Signal Analyzer (Tektronix CSA803) through a 20 GHz sampling head (Tektronix SD-26), which performs the sampling measurements on which we base our statistical studies. In addition to this fast detection equipment, we also employ an 8 GHz photodetector (Hamamatsu C4258) to receive the portion of the beam that passes through the beamsplitter after reflecting off the external cavity mirror. This signal is amplified and viewed on an oscilloscope. By using this configuration, we can observe the slower-scale LFF behavior while simultaneously maximizing the power incident on the fast photodetector. This is crucial, because a limiting factor in the measurements of this experiment is the baseline noise of the SD-26 sampling head, which becomes significant as compared to the optical signal near laser threshold. It is not possible to use a microwave amplifier to increase the signal, because necessary dc information would be lost. However, we note that accurate low-pump measurements can be made with the streak camera experiment, described in Sec. III B, which allows us to probe this regime. To examine the optical mode structure of the laser emission, we place a removable mirror after the Faraday isolator and redirect the beam to a nonconfocal Fabry-Perot analyzer (Newport SR-240 SuperCavity). The free-running external cavity laser system displays multilongitudinal mode operation. Therefore, when we wish to study the single-mode case, we insert an intracavity etalon (free spectral range$=1029$ GHz, finesse$=15.8$) between the beamsplitter and the mirror. Finally, the optical feedback level is controlled by inserting a polarizer and rotatable quarter-wave plate in the cavity.

To measure single-mode LFF statistics, we first adjust the etalon and verify with the optical spectrum analyzer that only one longitudinal mode is active. We then direct the beam to the Schottky detector and store $20k$ total data points in the CSA803's memory, as well as a baseline noise measurement with the laser beam blocked. The sampling scope is triggered internally, so that the measurement times are not correlated to the laser's behavior. The minimum time interval between two subsequent measurement points is 5 μs, thus there is ample time between measurements for the system to decorrelate completely. While taking data, we visually confirm the presence of the expected behavior using the slower photodetector and oscilloscope. Once all the data are stored, we immediately measure the P-J curve of the system to determine the threshold reduction. The data are then downloaded from the CSA to a personal computer and stored on hard disk for analysis. This procedure is repeated for various pump current levels.

The procedure is simplified when the laser is free to run in multiple longitudinal modes. In this case, there is no need to remeasure the threshold reduction at each pump current setting. Therefore, we simply store $20k$ data points and one baseline set for all selected pump currents (still viewing the behavior on the oscilloscope), and then measure the P-J

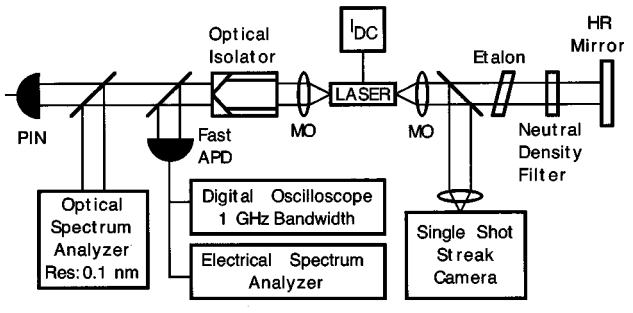

FIG. 3. Setup for the streak camera experiment.

curve once. We then examine the optical mode structure for the system, recording the number of participating longitudinal modes at each pump current value.

B. Streak camera experiment

The setup of the streak camera experiment, depicted in Fig. 3, allows us to extract statistical information about the dynamics of an external cavity semiconductor laser even for low laser intensities close to threshold, and to record single-shot intensity time series with a bandwidth of more than 50 GHz. Using this experimental technique, we can corroborate and complement the results of the fast sampling scope experiment described above. The laser diode used in the streak camera experiment is a Hitachi HLP1400 of channeled-substrate-planar structure (CSP) with uncoated facets. We use a different type of laser diode in this setup to assure that the obtained results are independent of the particular type of laser. The HLP1400 is driven by an ultralow noise current source; the temperature is stabilized to better than 0.01 K. The emission wavelength of the solitary laser is 840 nm, and its threshold current is 57.2 mA. The laser beam is collimated by microscope objectives (MO); the optical isolator shields the laser from unwanted optical feedback. The external cavity consists of a high-reflection mirror with an interferometric flatness of $\lambda/200$, a neutral density filter to control the amount of optical feedback, and, optionally, an intracavity etalon with a transmission bandwidth of 5 nm to restrict the dynamics of the system to a single longitudinal diode mode. The round trip time of the light in the external cavity is $\tau = 3$ ns.

This experimental setup allows the simultaneous measurement of the intensity time series, the power spectrum, and the optical spectrum of the laser. In particular, the intensity time series of the system is measured on three different levels of temporal resolution in order to account for the wide range of time scales present in its dynamics. First, the time-averaged intensity is monitored by a *p-i-n* photodiode in order to determine the *P-J* characteristics and, thus, the threshold reduction due to the optical feedback. Second, the intensity dynamics are detected by a fast avalanche photodiode (APD) with a bandwidth larger than 3 GHz. The power spectrum of the APD signal is measured by an electrical spectrum analyzer. The intensity time series of the APD signal is low-pass filtered with a cutoff frequency of 1 GHz and detected by a fast digital oscilloscope of the same bandwidth. Third, we investigate the intensity dynamics of the system with a single-shot streak camera. A beam splitter directs 50% of the light intensity emitted by the laser onto the entrance slit of the streak camera. The huge bandwidth of the streak camera device from dc to more than 50 GHz allows us to take single-shot time traces with the full temporal resolution of the fast pulsing underlying the dynamics displayed by the oscilloscope. The length of the recorded time series is limited to 7.3 ns. Furthermore, the light intensity is sufficient to record the intensity dynamics of the system with a low measurement noise even for low injection currents close to threshold. The optical spectrum is monitored continuously by a grating spectrometer with a resolution of 0.1 nm resolving the longitudinal diode modes. This guarantees that single-mode operation using the intracavity etalon is maintained throughout the entire measurement.

Performing the experiment, we record 20 arbitrarily triggered streak camera single shots of the intensity dynamics for each investigated injection current. From this, we obtain more than 20 000 data points which are stored for a subsequent statistical analysis. We repeat the experiment, both for the multimode and single-mode cases, for various injection currents from threshold up to the fully developed coherence collapse regime.

IV. RESULTS

In this section, we present the results of our experimental and numerical investigation of the picosecond intensity statistics of semiconductor lasers subject to delayed optical feedback. We compare intensity statistics obtained from numerical simulations of the LK equations to experimental results obtained from both experiments. In Sec. IV A, we compare the probability density distributions recorded for single and multimode emission of the laser. In both cases, and for all pump levels, the experiments reveal continuously decaying probability density distributions with long tails at high intensities. Our findings are supported by numerical simulations which yield very similar probability density distributions. In Sec. IV B, we show that gain saturation can lead to qualitative changes of the probability density function.

A. Single-mode versus multimode results

Figure 4 displays numerical and experimental results for both single-mode and multimode emission of the laser. For ease of comparison, all data are shown in the form of probability densities of the total laser intensity I. That is, the vertical axis represents the density $D(I)$, where $P(I) = D(I)dI$ is the probability that a given intensity measurement will fall between the values of I and $I+dI$, as dI becomes small. We approximate $D(I)$ with histograms of the intensity data, scaled to the total number of points and bin width. The horizontal axis is scaled to the average intensity I_{av}.

Numerical results are shown in Figs. 4(a) and 4(b) for single-mode and multimode cases, respectively. All numerical probability densities are derived from $32k$ points, calculated as described in Sec. II. These two graphs show $D(I)$ as a function of pump current, relative to the solitary threshold value J_{th}. Three pump values are shown: one very close to the solitary threshold, one moderate, and one well above threshold ($J/J_{\mathrm{th}} = 1.01$, 1.10, and 1.50, respectively). The optical feedback η is such that the laser threshold is reduced by 5%, and the gain saturation parameter is set at zero (we investigate nonzero ϵ in the next section). In each case, the probability density shows a peak at low intensity and rolls off at several times the average. A probability density of this type is expected for a pulsating laser with irregular, fully modulated pulses of a peak power of several times the average intensity. As the pump current increases, the roll-off tends to occur at lower normalized intensity.

Figures 4(c) and 4(d) show experimental probability distributions for the single-mode and the multimode case, respectively, obtained from the experiment using the Sharp LT015MD laser and the fast sampling scope. The fast sampling scope allows statistical measurements with picosecond

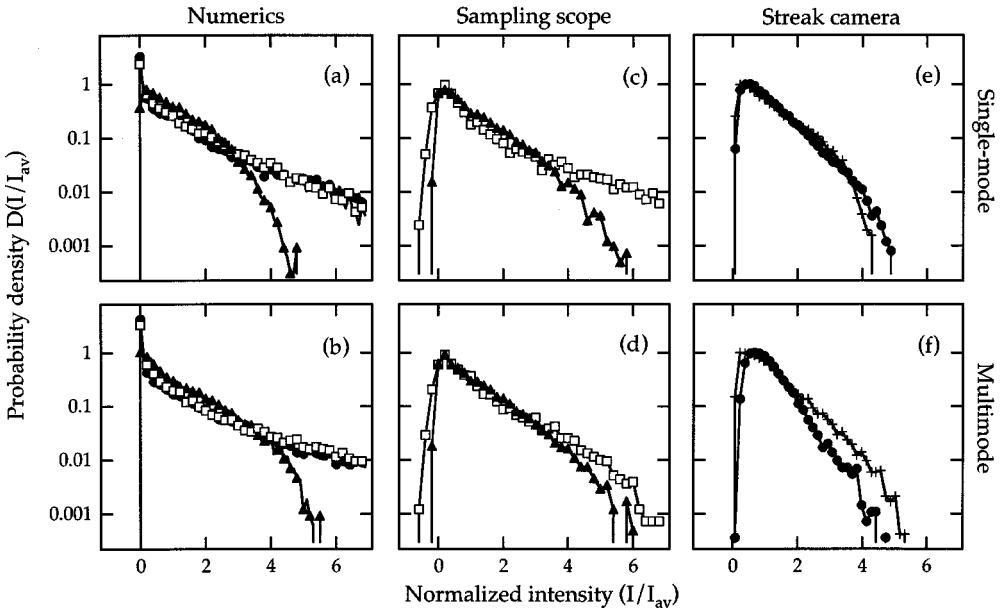

FIG. 4. Experimentally and numerically obtained probability density distributions. (a),(b) Numerical results for the single and multimode case, respectively, for three different injection currents: circles correspond to $1.01J/J_{\mathrm{th}}$, open squares to $1.10J/J_{\mathrm{th}}$, and triangles to $1.50J/J_{\mathrm{th}}$. (c),(d) Results of the fast sampling scope experiment for the single and multimode case, respectively, for two different injection currents: open squares correspond to $1.10J/J_{\mathrm{th}}$, triangles to $1.50J/J_{\mathrm{th}}$. (e),(f) Results of the streak camera experiment for the single and multimode case, respectively, for two different injection currents: circles correspond to $1.01J/J_{\mathrm{th}}$, crosses to $1.05J/J_{\mathrm{th}}$.

resolution of very long time series spanning several intensity dropouts. Two data sets derived from $20k$ points are shown, for pump currents 10% and 50% above solitary threshold. The features of these experimental data are in good agreement with the numerical findings: the maximum of the probability density is at very low intensity, clearly below the average intensity; then the probability density rolls off at high intensities up to several times I_{av}. The probability density distributions obtained from this experiment show no qualitative differences between single and multimode emission of the laser. The nonzero probabilities measured for small negative intensities are spurious; they result from the digitizer noise floor smearing out the low-intensity peak. Measurements made with the laser beam blocked provide a quantitative measure of this noise. Assuming normal distributions, their standard deviations at 10% and 50% above threshold are approximately $\sigma = 0.15I_{\mathrm{av}}$ and $0.04I_{\mathrm{av}}$, respectively.

In comparison, we have recorded probability distributions under similar experimental conditions using the streak camera setup and the HLP1400 laser. Exploiting the sensitivity of the streak camera system, we are able to record probability distributions even for the low intensities close to solitary laser threshold. Figures 4(e) and 4(f) show the probability distributions obtained from the streak camera experiment for pump currents 1% and 5% above solitary threshold, respectively. Figure 4(e) shows the single-mode emission case, Fig. 4(f) the multimode case. Again, the probability distributions are similar to the previously presented experimental and numerical results. Moreover, we obtain very similar intensity distributions for single and multimode emission case. The obtained probability distributions exhibit a peak at very low intensity and decay continuously to about four times the average intensity.

Although the roll off tends to occur at lower intensities for the HLP1400 laser, the probability distributions are in very good qualitative agreement with the results for the LT015MD laser presented in Figs. 4(c) and 4(d). It is quite plausible that the small quantitative differences between the results of the two experiments are due to physical differences between the lasers used. For example, both facets of the Hitachi HLP1400 are uncoated, whereas the Sharp LT015MD has one high-reflectivity facet and one with a partial antireflection coating. Other material parameters of various models and designs of semiconductor lasers are known to have wide variations as well, and could affect the intensity statistics of the laser dynamics.

To summarize, the numerical simulations of the LK equations show characteristic intensity probability distributions. The results of both the fast sampling scope experiment and the streak camera experiment are in good agreement with these numerical predictions. Our results demonstrate that neither changing the number of optical modes involved in the laser emission nor varying the pump current level necessarily leads to significant changes of the picosecond intensity probability distributions. In the following section, however, we identify physical mechanisms that can introduce qualitative changes to the probability distributions.

B. Effects of gain saturation and coexisting attractors

Although the presence of multiple optical modes has little effect on the probability distributions, we find that gain saturation and coexisting attractors can lead to qualitative changes. The effect of gain saturation is most pronounced for pump currents well above threshold, where larger laser intensities would be expected to enhance saturation effects. For pump currents close to solitary threshold, the coexistence of

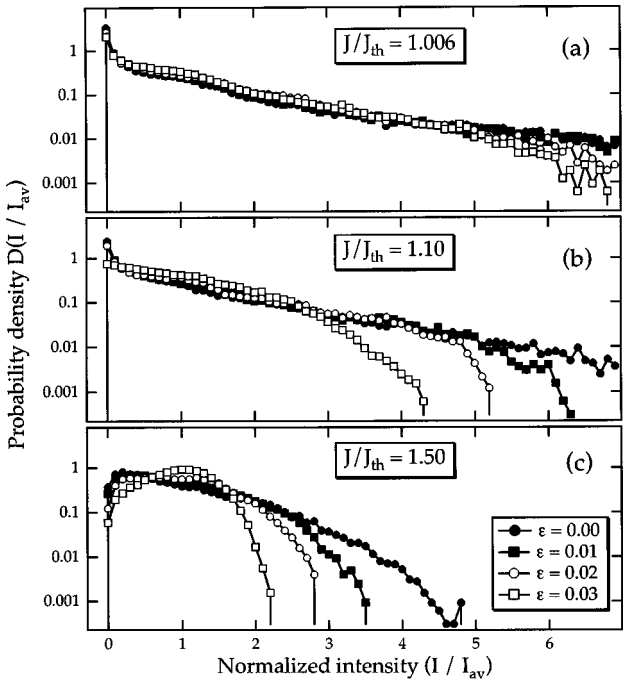

FIG. 5. Numerical probability density distributions for three different injection currents and four different values of the gain saturation parameter ϵ obtained for the single-mode case.

LFF with a stable emission state may also lead to qualitative changes of the probability distributions.

We study the effects of gain saturation by numerical means only, since it is a fixed material parameter in a given laser (although there can be a wide variation between different devices). These results are presented in Fig. 5, which shows probability distributions as a function of the gain saturation parameter, for three different pump strengths. The data shown are calculated using the single-mode LK model, but we have verified that the same results occur in the multimode case as well. Additional calculations (not shown) indicate that the distributions do not depend sensitively on the ratio of the cross-coupling strength C to self-saturation strength k in the multimode model (see Sec. II). In Fig. 5(a), the system is pumped near solitary threshold ($J/J_{\rm th}=1.006$), and ϵ is varied from 0.00 to 0.03. The effects of ϵ are very slight in this case, only becoming noticeable in the high-intensity tails of the distributions. In Figs. 5(b) and 5(c), where $J/J_{\rm th}=1.1$ and 1.5, respectively, the role of ϵ becomes much more pronounced. Larger values of ϵ cause the high-intensity tail to roll off quickly, strongly enhancing the trend that occurs at higher pump currents. Of special interest is the case for which $J/J_{\rm th}=1.5$ and $\epsilon=0.03$. For these parameters, the probability distribution changes qualitatively; it is no longer peaked near zero intensity, but instead shows a prominent maximum near $I_{\rm av}$. We note that this distribution shape is similar to those observed in other experiments [10]. We emphasize that the values of ϵ that are studied here are physically quite plausible, especially given the wide variations that occur between lasers for this parameter. Typical experimentally measured values of ϵ range from approximately 0.005 to 0.025 [28,29].

A second mechanism that can change the probability distributions is the coexistence of the LFF state with stable emission on a single high-gain external-cavity mode. Recently, it has been demonstrated that the dynamics may hop between these two states [33] in certain regimes, particularly at low pump currents. In such a case, the probability distribution will not be a true representation of the pure LFF statistics, but instead will reflect the combination of LFF with stable emission. In numerical simulations of probability distributions under coexistence conditions, we find a strong peak near the average intensity, corresponding to the stable emission state, which is superposed on the background of the exponentially decaying LFF distribution. We note that both gain saturation effects and coexisting attractors are accounted for by the LK model.

There is some evidence that the picosecond pulsations may become more frequent and smaller in peak intensity, possibly displaying antiphase behavior in the multimode case, under the conditions of very strong optical feedback and very long time intervals between the dropouts. This may contribute to probability distributions more like those shown in Fig. 5(c). Furthermore, we note that multimode action may enhance the effect of ϵ, since some researchers attribute gain saturation in part to longitudinal mode beating that modulates the refractive index [30–32].

V. SUMMARY

We have presented a detailed experimental and numerical investigation of the statistical properties of the intensity dynamics of external cavity semiconductor lasers operating in the LFF and CC regimes. By using two different, complementary experimental techniques, we have addressed all relevant time scales in a study of the role of multiple-optical mode operation in LFF dynamics. The statistics we obtain from single-mode and multimode configurations are essentially indistinguishable in both experimental and numerical investigations. While these results do not preclude the possibility that multimode dynamics may in some cases contribute to the LFF dynamics, they are evidence that the presence of multiple optical modes is not truly fundamental to LFF mechanisms. This supports the assertion that the usual single-mode Lang-Kobayashi equations are sufficient to capture the essence of the phenomena in this region. Furthermore, we have demonstrated that the effects of gain saturation and coexisting attractors can strongly change the probability distribution, over a modest and physically reasonable range of parameter values. The effect of gain saturation is strongest for moderately strong pump currents, as would be expected for higher average laser intensities. Gain saturation effects and coexisting attractors may be able to reconcile disparities in various experimental observations.

ACKNOWLEDGMENTS

D.W.S. and A.H.-A. gratefully acknowledge the National Research Council and the U.S. Air Force Office of Scientific Research for their support of this work. T.H., I.F., and W.E. acknowledge the Deutsche Forschungsgemeinschaft for funding within the Sonderforschungsbereich 185 Nichtlineare Dynamik. The authors would like to thank Julian Cheng, Drew Aldunio, and Chris Hains for access to and assistance with the CSA803.

[1] R. Lang and K. Kobayashi, IEEE J. Quantum Electron. **QE-16**, 347 (1980).
[2] F. Mogenson, H. Oleson, and G. Jacobsen, Electron. Lett. **21**, 696 (1985).
[3] H. L. Wang, M. J. Freeman, and D. G. Steel, Phys. Rev. Lett. **71**, 3951 (1993).
[4] C. Risch and C. Voumard, J. Appl. Phys. **48**, 2083 (1977).
[5] R. W. Tkach and A. R. Chraplyvy, J. Lightwave Technol. **LT-4**, 1655 (1987).
[6] M.-W. Pan, B.-P. Shi, and G. R. Gray, Opt. Lett. **22**, 166 (1998).
[7] D. Lenstra, B. H. Verbeek, and A. J. den Boef, IEEE J. Quantum Electron. **QE-21**, 674 (1985).
[8] G. H. M. van Tartwijk, A. M. Levine, and D. Lenstra, IEEE J. Sel. Top. Quantum Electron. **1**, 466 (1995).
[9] I. Fischer, G. H. M. van Tartwijk, A. M. Levine, W. Elsäßer, E. Göbel, and D. Lenstra, Phys. Rev. Lett. **76**, 220 (1996).
[10] G. Huyet, S. Hegarty, M. Giudici, B. de Bruyn, and J. G. McInerney, Europhys. Lett. **40**, 619 (1997).
[11] D. W. Sukow, J. R. Gardner, and D. J. Gauthier, Phys. Rev. A **56**, R3370 (1997).
[12] J. Sacher, W. Elsäßer, and E. O. Göbel, Phys. Rev. Lett. **63**, 2224 (1989).
[13] C. H. Henry and R. F. Kazarinov, IEEE J. Quantum Electron. **QE-22**, 294 (1986).
[14] J. Mørk, B. Tromberg, and P. L. Christiansen, IEEE J. Quantum Electron. **QE-24**, 123 (1988).
[15] T. Sano, Phys. Rev. A **50**, 2719 (1994).
[16] A. Hohl, H. J. C. van der Linden, and R. Roy, Opt. Lett. **20**, 2396 (1995).
[17] B. Tromborg, J. Mørk, and V. Velichansky, Quantum Semiclassic. Opt. **9**, 831 (1997).
[18] G. Huyet, S. Balle, M. Giudici, C. Green, G. Giacomelli, and J. R. Tredicce, Opt. Commun. **149**, 341 (1998).
[19] G. Vaschenko, M. Giudici, J. J. Rocca, C. S. Menoni, J. R. Tredicce, and S. Balle, Phys. Rev. Lett. **80**, 5536 (1998).
[20] H. Temkin, N. A. Olsson, J. H. Abeles, R. A. Logan, and M. B. Panish, IEEE J. Quantum Electron. **QE-22**, 286 (1986).
[21] G. Gray and R. Roy, Phys. Rev. A **40**, 2452 (1989).
[22] G. Gray and R. Roy, J. Opt. Soc. Am. B **8**, 632 (1991).
[23] A. Gavrielides, V. Kovanis, P. M. Varangis, T. Erneux, and G. Lythe, Quantum Semiclassic. Opt. **9**, 785 (1997).
[24] M. R. Alalusi and R. B. Darling, IEEE J. Quantum Electron. **QE-31**, 1181 (1995).
[25] G. P. Agrawal, IEEE J. Quantum Electron. **QE-23**, 860 (1987).
[26] C. B. Su, J. Schlafer, and R. B. Lauer, Appl. Phys. Lett. **57**, 849 (1990).
[27] C. Becher, E. Gehrig, and K.-J. Boller, Phys. Rev. A **57**, 3952 (1998).
[28] C. Masoller and N. B. Abraham, Phys. Rev. A **57**, 1313 (1998).
[29] J. Ye, H. Li, and J. G. McInerney, Phys. Rev. A **47**, 2249 (1993).
[30] M. Yamada and Y. Suematsu, J. Appl. Phys. **52**, 2653 (1981).
[31] G. P. Agrawal, Phys. Rev. A **37**, 2488 (1988).
[32] M. Ohtsu and Y. Teramachi, IEEE J. Quantum Electron. **25**, 31 (1989).
[33] T. Heil, I. Fischer, and W. Elsäßer, Phys. Rev. A **58**, R2672 (1998); I. Fischer, T. Heil, M. Münkel, and W. Elsäßer, Proc. SPIE **3283**, 571 (1998).